Characterization of a modular microfluidic section for seeded nucleation in multiphase flow

Cedric Devos [a‡], Elena Brozzi [a‡], Tom Van Gerven [a], and Simon Kuhn [a]*

[a] *KU Leuven, Department of Chemical Engineering, 3001 Leuven, Belgium*

[*] Email: simon.kuhn@kuleuven.be

[‡] *C.D. and E.B. contributed equally to this paper.*

KEYWORDS: Nucleation, microfluidic, seeding, crystallization, multiphase, continuous

ABSTRACT: We present a proof-of-concept modular nucleation section for seeded multiphase flow crystallization of an active pharmaceutical ingredient. The setup can be used in four different modes of operation (with and without off-line prepared seeds, with or without a stream of microbubbles). The setup is characterized to provide insights into the design and operation of crystallization processes. Firstly, the performance of the off-line continuous seeding platform is established via the seed delivery efficiency for constant and oscillatory flows. Secondly, the yield of seeded and unseeded crystallization is evaluated in the presence and absence of microbubbles. A statistically significant increase in the net crystal mass and net yield was measured when comparing unseeded and seeded crystallization, which can be attributed to the increased nucleation rates as a result of secondary nucleation. Thirdly, the clogging behavior of the continuous

microcrystallizer is discussed. Finally, also the crystal size distribution is analyzed: mean crystal size decreases for both single- and two-phase flow when seeds are introduced. The presence of microbubbles resulted in a higher net yield and slightly smaller crystals compared to single-phase flow. This work highlights the importance of a holistic characterization approach for continuous microfluidic crystallizers.

1. INTRODUCTION:

Crystallization is one of the most important separation and purification operations in the pharmaceutical industry [1], though it is inherently difficult to control. The most common equipment for crystallization processes is the batch crystallizer [2]. Poor mixing and dead-zones in such crystallizers result in bad process control and batch-to-batch variability [3]. With the objective of obtaining reproducible and scalable crystallization processes with large space-time yields, continuous crystallizers have become popular in recent years.

Continuous crystallizers can be divided in mixed suspension mixed product removal crystallizers (MSMPR) [4,5], continuous oscillatory baffled crystallizers (COBC) [6–10], and tubular flow crystallizers (TFC) [11]. Several recent reviews discuss the advantages of continuous crystallization in more detail [12–16], such as consistent production and no batch-to-batch variability. One type of TFC is the continuous microcrystallizer. Microcrystallizers have a small characteristic size, which results in very large surface-to-volume ratios. This leads to high mass and heat transfer rates when compared to conventional equipment, which improves control over cooling crystallization processes. Their main disadvantage is their low throughput, which is also a direct result of their small size. This does not prevent continuous microcrystallizers from being great tools for rapid (exploratory) screening and process development [17], in particular if the crystallization kinetics are sufficiently high, such that residence times can be short [18]. This makes

microdevices potentially attractive tools for the pharmaceutical industry to reduce the time-to-market. Moreover, they can be used for on-demand production of low dosage active pharmaceutical ingredients (API's) in an end-to-end manufacturing process. On-demand manufacturing aims at flexible, versatile and localized production of drug products to avoid reliance on complex supply chains [19,20] as an alternative to traditional large-scale batch manufacturing. Continuous microcrystallizers are ideal for this application, as it requires fast processes with a small footprint. Nevertheless, due to their low throughput continuous microcrystallizers cannot generally be applied directly for industrial production, where a throughput of 100 or even 1000 times as large is common [21]. A general overview of the scale-up possibilities for continuous microreactors was discussed recently in a review by Dong et al., with an emphasis on the numbering-up (or parallelizing) and scaling-out techniques [21].

Continuous microcrystallizers also suffer from other disadvantages, though. Due to the small scale, the flow is laminar, which causes weak convective mixing. In addition, the fluid velocity near the wall is low and solid particles may deposit in the TFC, causing channel clogging [22,23]. Both active (with the use of an externally applied force) and passive methods (without the use of any external forces except pumping) have been proposed to tackle clogging [23]. The most commonly applied passive method is two-phase flow [22,24]. Slug flow crystallizers, either gas-liquid (G-L [24–28]) or liquid-liquid (L-L [29,30]), have been used for several years. Slug flow is characterized by a dispersed phase with a characteristic size length that is larger than the channel diameter [31]. In continuous bubble flow crystallizers [32] the bubble diameter is smaller than the channel diameter. Even though this leads to a higher productivity without any major drawbacks compared to a slug flow crystallizer, bubble flow crystallizers have not yet been used as often. By using G-L instead of L-L flow, no additional complex downstream separation is required.

The most common active method to overcome channel clogging is the use of ultrasound (US) [33]. Sonication is also known to increase the nucleation rate [29,34] and as a result narrower crystal size distributions (CSD) are obtained [35,36].

Accurate control over crystallization processes requires control over both nucleation and growth. In continuous tubular crystallizers it is common to try decoupling the nuclei generation from the growth of those nuclei (e.g. [29,37]) by manipulating the supersaturation in different sections of the crystallizer. The "nucleation section" is usually kept at high supersaturation (or low temperature), to form nuclei. The "growth section" is generally operated at lower supersaturation (or higher temperature), to grow the largest and most stable nuclei, whilst dissolving the smallest nuclei.

Nevertheless, it remains impossible to know whether crystals do not grow in the nucleation section or whether no nucleation occurs in the growth zone [38]. Hence, complete decoupling is impossible and careful consideration of the nucleation section is of paramount importance in the design of continuous tubular crystallizers. It is important to consider the upper (too much growth, such that clogging occurs) and lower (no nucleation) supersaturation boundaries of the nucleation section.

Nucleation is intrinsically stochastic, which manifests itself in varying induction times in small volume crystallization. To reduce the reliance on the uncontrollable primary nucleation, nucleation optimization or minimization is necessary [39,40]. The addition of crystal seeds prior to the crystallization is one of the most used methods, in both research and industry [39,40]. Once sufficient seeds are present in the crystallizer, secondary nucleation becomes the dominating nucleation mechanism [38,41]. Seeding in TFCs, where seeds are constantly flushed out, is distinctly different than seeding in batch crystallizers, where seeds remain in the crystallizer for the entire duration of the process. For TFCs, a distinction must be made between in-line (or in situ) nuclei generation

(sometimes called self-seeded) crystallizers, in which nuclei are generated in the tubular crystallizer and no crystals are present at the inlet of the crystallizer, and off-line nucleation generation (or a seeded crystallizer), in which seed crystals are produced in an apparatus not directly connected to the tubular crystallizer and added at the start of the process.

In-line nuclei generators usually require an external stimulus [39]. The most common one is the use of an acoustic field [24,25,35,42,43]. Jiang et al. used an US probe to generate a localized zone for nucleation [24]. Similarly, Jordens et al. generated a localized zone for nucleation using a Langevin ultrasonic transducer [42]. Others have used an ultrasonic bath [25,43]. Fatemi et al. used controlled injection of inert microbubbles as an external stimulus [37]. Rimez et al. have used tube restrictions to increase the nucleation rate [44,45]. The main problem of such in-line seeding apparatuses is that they still inherently rely on primary nucleation. Decoupling nucleation and seeding allows for seeding crystals with defined properties (e.g., polymorph, surface chemistry, roughness, and size) that may not be easily obtainable with an in-line nuclei generator.

Delivery of a suspension of crystals and solution in the off-line approach is not straightforward, though, due to the tendency of the crystals to clog the channel or the connections. It is generally advised to continuously stir the feed solution and apply external actuation (e.g. an acoustic field) to the crystallizer to keep the solid seeds in solution and avoid settling [22]. It is important to consider the particle sizes and feed solution concentration for optimal delivery [22]. The addition of a suspension increases in complexity for decreasing diameters.

Table 1 gives a selected overview of continuous small-scale tubular crystallizers in literature. Only cooling crystallization is considered in this article. It shows that all continuous tubular microcrystallizers (except [37] and [44]) are millicrystallizers and that designs in the microcrystallizer range have been largely unexplored. The yield column in this table refers to the highest yield

(defined as the ratio of crystal product and theoretical yield) reported in the paper, which is highly dependent on the seed loading, compound, cooling profile, supersaturation, seed size, residence time, and other parameters. TFCs are often coiled to reduce the operational space, and to improve mixing through the induction of Dean vortices [46,47]. More recently, also coiled flow inverter (CFI) crystallizers have been used to further enhance the effects of coiling [46,48–50]. The usage of coiled crystallizers is discussed in the supporting information (S1. Coiled crystallizers in literature).

In this work, a continuous microcrystallizer for multiphase and seeded nucleation of paracetamol from an aqueous solution is developed. To contribute to the development of continuous microcrystallizers as tools for exploratory screening, two issues which hinder the use of their industrial application are addressed. Firstly, it is important to have a system with simple extensibility to validate various cases. In particular the possibility of seeding with offline prepared seeds is of value for the pharmaceutical industry. Secondly, thorough characterization of the system in terms of seed delivery, net yield, crystal size distribution, and clogging is essential for process understanding. This is illustrated by a discussion concerning the crystallization mechanisms in various modes of operation.

The setup consists of four modules: the first module (M1) is the tubular nucleation section itself. The second module (M2) is the delivery system for the undersaturated solution. The third module (M3) is the delivery system for a suspension of seeds. It includes a vertically mounted syringe pump, with a stirred and temperature-controlled syringe, and a seeding section, in which suspension and undersaturated solution are mixed. This seeding section is sonicated to keep the solids in suspension and prevent agglomeration. The temperature increase due to continuous sonication [33] is used to avoid nucleation in this module. The fourth module (M4) can be used to introduce microbubbles into the nucleation section. Four different cases can be therefore

investigated: seeded and unseeded single-phase flow, seeded and unseeded two-phase flow. The performance of the delivery system is evaluated in terms of net seed input (delivery efficiency), while crystallization of paracetamol is determined by the net output (or net yield), the clogging behavior and the CSD.

Table 1. Selected overview of TFCs in literature for cooling crystallization of organic molecules. (*) calculated based on results reported in the paper. The presented work is highlighted in the table.

	Nuclei generation	**Nucleation production**	**Compounds**	**Dimensions**	**Flow**	**Highest reported yield**
Present work (2022)	Off-line	Batch crystallizer and sieving	PCM in water	ID =1.0 mm, L = 60 cm	G-L bubbles	50 %
Méndez Del Río and Rousseau (2006) [51]	In-line	Tubular crystallizer	PCM in ethanol/methanol	ID = 1.6 mm, L = 7.62 m	Single-phase	N/A
Eder et al. (2010) [52]	Off-line	Batch crystallizer	ASA in ethanol	ID = 2 mm, L = 15 m	Single-phase	97 % (*)
Eder et al. (2011) [53]	Off-line	Batch crystallizer	ASA in ethanol	ID = 2 mm, L = 15 m	Single-phase	N/A
Eder et al. (2012) [25]	In-line	US-induced	ASA in ethanol	ID = 2 mm, L = 27 m	G-L slugs	N/A
Wong et al. (2013) [54]	In-line	Single crystal contact nucleation	Glycine, PCM in water	ID = 3.2 mm, L = 6.1 m	Single-phase	N/A
Jiang et al. (2014) [26]	In-line	Mixing hot and cold solution	LAM in water	ID = 3.1 mm, L = 15.2 m	G-L slugs	99 % (*)
Jiang et al. (2015) [24]	In-line	US-induced	LAM in water	ID = 3.1 mm, L = 15.2 m	G-L slugs	99 % (*)
Besenhard et al. (2015) [55]	Off-line	US-induced batch crystallizer	ASA in ethanol	ID = 2 mm, L = 15 m	Single-phase	N/A

Neugebauer and Khinast (2015) [28]	In-line	Mixing crystallization agent	Lysozyme in NaCl	ID = 2 mm, L = 13 m	G-L slugs	88 %
Jordens et al. (2017) [42]	In-line	US-induced	PCM in water	ID = 5 mm, L = 7 m; V_{batch} = 0.43 m^3	Single-phase	N/A
Hohmann et al. (2018) [47]	Off-line	Batch crystallizer and sieving	L-alanine in water	ID = 4 mm, L = 6.5 m	Single-phase	N/A
Rimez et al. (2018) [44]	In-line	Cooling and tube restrictions	Brivaracetam in IPAc	ID = 1.0 mm, L = 7 m	Single-phase	N/A
Han et al. (2018) [43]	Off-line	Batch crystallizer (US-induced)	$CuSO_4$, K_2SO_4, $C_8H_6O_4$ in water	ID = 4 mm, L = 12, 18 m	Single-phase	79 %, 24%, 63 %
Fatemi et al. (2022) [37]	In-line	Microbubbles induce heterogeneous nucleation	PCM in water	ID = 1.0-2.0 mm, L = 60 cm, 1.4, 4.0, 8.0 m	G-L bubbles and slugs	71 %
Termühlen et al. (2021) [27]	Off-line	Batch crystallizer and sieving	L-alanine in water	ID = 3.2 mm, L = 7, 13.25, 26.5 m	G-L slugs	83 %

2. MATERIALS AND METHODS:

2.1 Preparation of the stock solution Paracetamol (PCM, acetamidophenol, 98 % purity) from Acros Organics was used to prepare 300 mL stock solutions by dissolving 7.32 g (measured on a VWR LP-2102i balance with a precision of 0.01 g) in 300 mL of distilled water, which corresponds to a solution saturated at 40°C, according to the solubility data [56]. All solutions were filtered (qualitative filter, grade 303, particle retention range 5-13 μm) prior to usage. The stock solution is stored at 80 °C on a stirred heating plate.

2.2 Preparation of the seed suspension Crystal seeds are produced in a batch cooling crystallization process. A solution is prepared by dissolving 14.5 g of PCM in 300 mL of distilled water, which corresponds to a solution saturated at 60 °C [56]. This solution is filtered (qualitative filter, grade 303, particle retention range 5-13 μm) and stored at room temperature (20-22 °C) for two days. Then, solid crystals are filtered (qualitative filter, grade 303, particle retention range 5-13 μm) from the solution and dried. The crystals are pestled and sieved twice (<75 μm, <56 μm, VWR sieve). It is advised in literature to feed seeds that are already wetted in a suspension [40]. Hence, the same suspension is prepared at the beginning of every experiment, with a weight concentration of 0.8 g seeds / 100 mL of stock solution, and stored at 40-45 °C. The seed suspension is then retracted using a syringe. We assumed that dissolution in the syringe is negligible during the first 10 min.

2.3 Experimental setup The experimental setup consists of four modules, as shown in Figure 1. Table 2 gives an overview of the different modules and the operating parameters that are studied. The first module (M1) is the microcrystallizer that serves as a nucleation section. It is a 60 cm horizontal glass capillary (CM Scientific, ID = 1.00 mm, OD = 1.20 mm, $\pm$ 0.1 mm). The crystallizer is submerged in a temperature-controlled water bath, which is controlled by a chiller

(Unichiller, Huber Kältemaschinenbau AG), to generate supersaturation (S). The supersaturation is approximated here as the ratio of the concentration at a certain temperature and the equilibrium concentration at that temperature. The flow rate through the crystallizer is fixed at 2 mL/min in this work, which results in a residence time of 14 s, but can be easily changed in future experiments.

Module 2 (M2) is the solution delivery module, which pumps the temperature-controlled undersaturated liquid with a positive displacement pump (M6, VICI). The temperature of the feed solution is chosen such that the inlet of the microcrystallizer is exactly at the saturation level (40 °C).

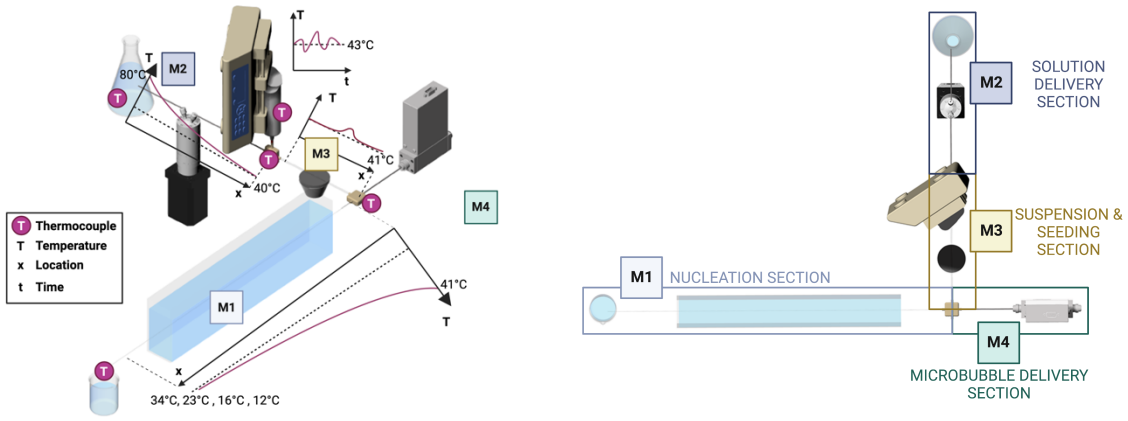

(a) (b)

Figure 1. Schematic overview of the setup from a (a) perspective view, and a (b) top view, with the different modules highlighted: M1 the temperature-controlled nucleation section, M2 the solution delivery system, M3 the suspension delivery and seeding section, and M4 the microbubble delivery system.

Module 3 (M3) is the suspension delivery module for seeded crystallization experiments. It consists of two parts: the syringe pump and the seeding section. The seeding section, in which a

mixture is formed by a saturated solution and suspended PCM seeds, is a 15 cm borosilicate glass tube (ID = 1.6 mm, OD = 3.0 mm, ± 0.1 mm) glued onto a Langevin-type transducer (OD = 50 mm). The inlet of the seeding section is connected to a vertical syringe pump (KR analytical), which injects the seed suspension, and a positive displacement pump (M6, VICI), which pumps the PCM solution. The outlet of the seeding section is connected in a 90° angle to the tubular nucleation section (M1).

Table 2. Overview of the different modules, their function. operating and characterized parameters.

Module	Function	Operating parameter	Characterized parameter
M1	Temperature-controlled nucleation section	Supersaturation	Net yield, CSD, clogging
M2	Solution delivery section	Flow rate (oscillation)	N/A
M3	Suspension delivery section	US power and seed loading	Delivery efficiency
M4	Microbubble delivery section	Single- or two-phase flow	N/A

To prevent nucleation of new crystals or dissolution of seeds in the syringe (TERUMO Japan, 10 mL, 15.80 mm), the temperature is controlled using two flexible electrical heating elements (KHLVA-0504/10, OMEGA). To ensure suspension of the seeds in the syringe, the PCM seeds solution is stirred using a PTFE stirring magnet and a vertically mounted magnetic stirrer (HI 180, Hanna Instruments). The flow rate of the PCM saturated solution and the seed suspension is respectively 1.5 mL/min and 0.5 mL/min. Hence, the cumulative flow rate through the seeding section is 2 mL/min.

To keep the seed crystals in suspension and prevent clogging, ultrasound (US) is applied using the Langevin transducer. It is operated at its resonance frequency (40.2 kHz). A waveform generator (Keysight 33500B) and power amplifier (EI, RF 2100 L, 100 W) are used to drive the transducer. The transducer is operated at 4 W (see section 2.4). No visible cavitation occurred in the seeding section. The heat generation due to the US is used to keep the seeding section around the saturation temperature (i.e. 40 ± 1 °C), and is therefore not a source of waste, as is often the case. The temperature is measured with thermocouples both at the inlet and outlet of the seeding section (OMEGA, SC-GG-K-30-36 and RS PRO, 110-4482) connected to a thermometer (HH374, OMEGA 4-channel data logger thermometer (accuracy ± 0.1 % + 0.7 °C)). The experimentally measured temperatures in the seeding section and the position of the thermocouples in the system are shown in the supporting information (S2. Temperatures measurements). A schematic overview of the setup with the different temperature profiles is also included in the supporting information (S2. Temperatures measurements).

Module 4 (M4) is the microbubble delivery module for two-phase flow experiments. Using this module, it is possible to inject N_2-microbubbles in a controllable manner into the microcrystallizer using a small silica-infused needle (ID = 20 μm, OD = 375 μm, L = 5 cm, Polymicro Technologies), as described and characterized by Fatemi et al. [32]. The gas flow rate is fixed at 0.05 mL/min for all experiments using a mass flow controller (Bronkhorst, EL-FLOW), which results in 0.13 mm^2/mm^3 bubble surface area per unit volume of reactor [32]. For single-phase flow nucleation experiments, this module is removed from the setup.

The stability of the bubble flow downstream in the microcrystallizer is not affected by sonication at 4 W in the seeding section. The pulse-free flow provided by the piston and syringe pump is a requisite for obtaining a stable bubble flow. Moreover, the importance of flow oscillations on the

stability of the two-phase flow was also recognized by Jiang et al. [26]. To prevent solids clogging in the connections between the different modules, the connections (IDEX, PEEK) are modified to an ID of 5.0 mm.

2.4 Experimental characterization of the suspension delivery section (module M3) To find the optimal operating power of the US transducer, the effect of varying US powers (2, 4 and 6 W) on the solid deposition and on the downstream flow in the nucleation section (M4) is characterized. The suspension inside the seeding section is recorded (500 frames per second (fps)) with a high-speed camera (Photron FASTCAM Mini UX100, resolution 1280 pixel x 480 pixel) equipped with a microlens (NAVITAR 1-50486).

Jordens et al. demonstrated that crystal breakage occurs at low US frequencies [42]. To evaluate the effect of seed breakage in the seeding section, the effect of different US powers on the CSD is measured at the outlet of the seeding section (module M3). Samples are collected at the outlet of the seeding section in a stirred batch at ambient temperature, and the CSD is analyzed directly at the outlet of the seeding section with a laser diffractometer (Malvern Mastersizer 3000).

2.5 Experimental characterization of the continuous crystallizer (module M1) Prior to the start of an experiment, the entire setup is cleaned using hot water, to remove solid deposition on the walls of the nucleation and seeding section. Then, the experiment is started. Every experiment takes 8 min, but no samples are collected during the first 2 min. Then, the outlet product of the microcrystallizer is filtered (MF-Millipore, MCE membrane filter, 0.22 μm) using a vacuum pump (VP 100 C vacuumbrand, VWR) to prevent further growth or nucleation on the filter. These filters are dried overnight at ambient temperature, and measured before and after filtering using a Mettler Toledo XS105 Dual Range balance with a precision of 0.01 mg. The weight increase is then used to characterize the delivery efficiency and net yield (as discussed in section 2.6). The seeds inlet

mass is determined experimentally by collecting the sample at the inlet of the crystallizer, prior to any onset of crystallization. The suspension flowing through the microcrystallizer is recorded with the high-speed camera equipped with the microlens, at 500 fps. The microchannel is illuminated using a light source (SCHOTT KL 2500 LED). Both the seed and product crystals are analyzed as discussed in section 2.7.

2.6 Delivery efficiency and net yield The delivery efficiency is defined as the ratio of the mass of crystals measured at the inlet of the microcrystallizer (where no crystallization has occurred yet) and the theoretical mass of seed crystals that is injected into the seeding section, as is shown in eq. 1. Whilst a delivery efficiency of 100% is desirable, where every seed injected into the seeding system enters the microcrystallizer, this is practically not feasible in microfluidic systems. Solids tend to remain in the seeding section and accumulate in the connections between the different sections. In addition, some crystals may dissolve due to localized temperature hotspots in the syringe or seeding section.

$$\text{Delivery efficiency } [\%] = \frac{m_{\text{seeds inlet}}}{m_{\text{seeds injected}}} \cdot 100 \quad (1)$$

The net yield of the system is defined as the ratio of the net crystallization that takes place in the microcrystallizer to the theoretical mass of crystals that can crystallize. Eq. 2 is used to calculate the net yield.

$$\text{Net yield } [\%] = \frac{m_{\text{crystals outlet}} - m_{\text{seeds inlet}}}{m_{\text{crystallize,theor}}\,(S)} \cdot 100 \quad (2)$$

2.7 Crystal size distribution analysis The dried (0.22 μm) filters are further analyzed under the microscope (Nikon SMZ25 Stereoscopic Zoom Microscope). The images were analyzed manually and randomly using ImageJ software, in order to obtain the number-based (Feret diameter) CSD. For every condition at least 500 crystals were recorded. From the microscopy pictures it is evident

that all crystals were monoclinic form I. Then, the crystals are scraped off the filter and the collected sample is analyzed using a laser diffractometer (Malvern Mastersizer 3000), in order to obtain the volume-based CSD. To prevent dissolution or growth of crystals, the cell is filled with approximately 6 mL of PCM solution saturated at 21 °C. The cell is stirred at 1500 rpm for all experiments, which does not result in measurable breakage of the crystals. Each condition is measured three times, and only the mean CSD is reported.

3. RESULTS AND DISCUSSION:

The continuous microcrystallizer setup is characterized in terms of delivery efficiency, net yield, clogging behavior and CSD. The first section focuses on the solid transport of the off-line prepared seeds with ultrasound and its effects on the delivery efficiency. The second section describes the net yield that is obtained in the continuous microcrystallizer for the different modes of operation. In the third section the clogging behavior is evaluated. The final section shows the effect of the different modules on the crystal size distribution.

3.1 Delivery efficiency

Delivery efficiency (as defined by eq. 1) is mainly determined by the transport of the seed suspension through the seeding section (module M3). US is used in this section to improve solid handling [57]. Figure 2 shows the effect of varying US powers in the seeding section (Module M3). In the silent case, the seeds deposit on the walls along the entire radial direction and only a low number of crystal seeds passes through the seeding section. Sonication causes the seeds to remain suspended and detached from the wall, such that more seeds flow through the seeding section. The lowest number of seeds deposited onto the channel is obtained at the applied power of 6 W. However, mechanical vibrations from this level of applied ultrasound power causes the downstream bubble flow in the nucleation section to become unstable. Unstable bubble flow

results in distorted bubbles, bubble coalescence, time-dependent bubble generation and variations in bubble size. Furthermore, with the purpose of controlling the temperature in the seeding section (to avoid seed dissolution caused by hotspots in the vicinity of the ultrasonic transducer) a lower applied power of 4 W is chosen.

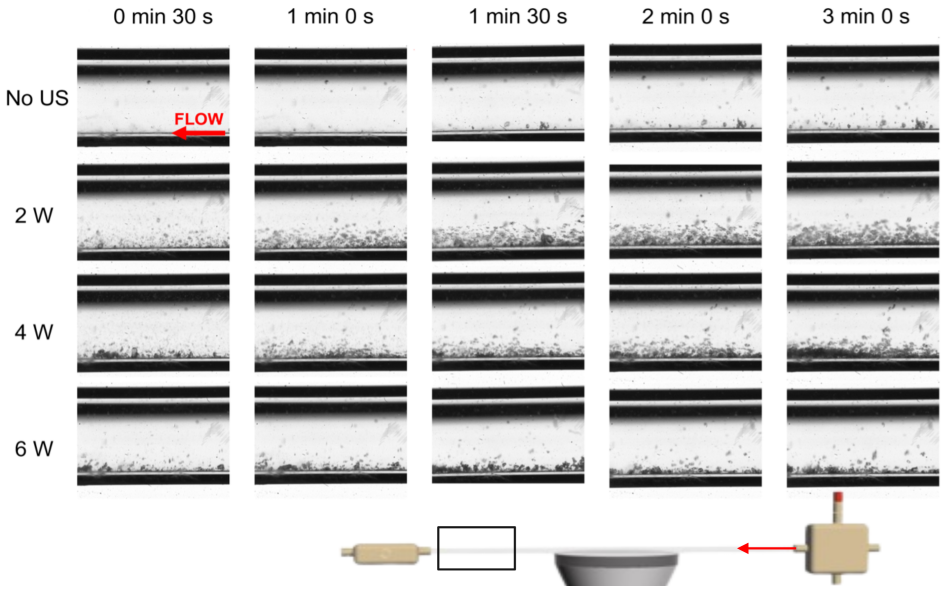

Figure 2. Images of the suspension in the seeding section (M3) over time for different applied US powers at the same seed loading. The field of view of the camera is indicated.

The delivery efficiency of the setup without the microbubble delivery module (M4) is higher (47%), than with the module incorporated (38%). This can be explained by the presence of the silica capillary in the microcrystallizer, that is a prerequisite for obtaining a bubble flow, which causes approximately 40% of the microcrystallizer inlet to be blocked. This is graphically shown in Figure 3 (b). Without module M4 installed, the nucleation unit inlet is larger, and more seeds can pass. These results illustrate the importance of analyzing not only the outlet, but also the inlet of the different sections in continuous crystallization setups.

Oscillating the flow rate in two-phase flow, whilst keeping the (mean) cumulative flow rate constant, increased the delivery efficiency to a value similar to the single-phase case, as shown in

Figure 3 (a). Details concerning the oscillating flow can be found in the supporting information (S7. Oscillating flow). The solid loading used in this work is considered high according to literature [40,47,58], especially for a continuous setup. The seed loading used in this work is discussed in more detail in the supporting information (S3. Solid loading). Lowering the seed loading would result in an increase in the delivery efficiency to values above 50%.

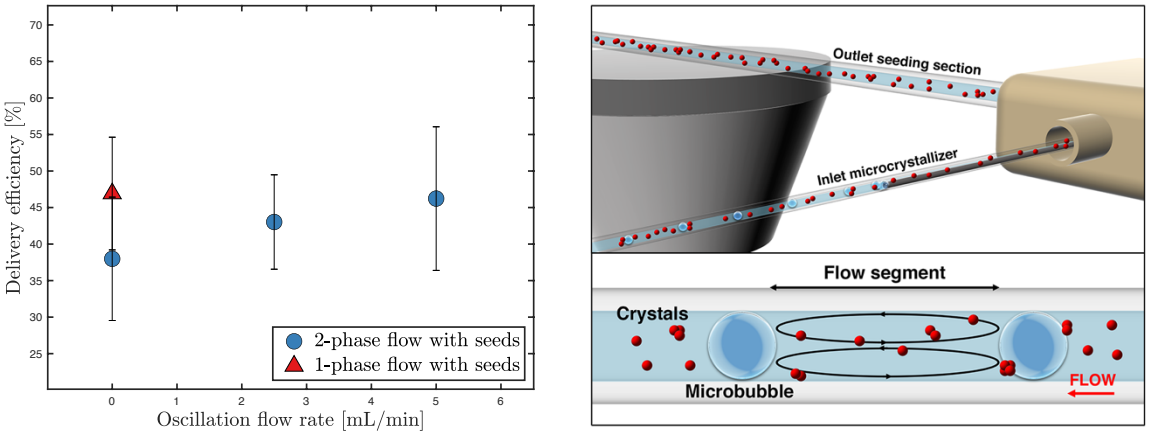

(a) (b)

Figure 3. (a) Delivery efficiency as a function of the flow rate of the pulse [mL/min]. The total cumulative flow rate is constant at 2 mL/min. (b) [TOP] Graphical representation of the setup with both modules M3 and M4 installed. [BOTTOM] Streamlines in the microcrystallizer. Figure adapted with permission from reference [59]. Copyright 2014 John Wiley and Sons.

3.2 Net yield

To determine the optimal condition for high (net) crystal yield the four operational modes are analysed for different supersaturations (1.22, 1.76, 2.20, 2.45). The net crystal mass that is obtained at the outlet of the crystallizer is shown in Table 3. At low supersaturations (S = 1.22) we see no increase in the net crystal mass for single-phase flow with seeding compared to without seeding. Similar values are obtained for the experiments without seeds and two-phase flow. We hypothesize that for low supersaturations and low residence times the seed crystals and the small nuclei that

are formed in the microcrystallizer due to heterogeneous or secondary nucleation do not have a relevant impact on the weight of the filter compared to the unseeded case. Moreover, noticeable crystallization occurs at the back of the filter in every experiment, due to the accumulation of supersaturated solution during filtration, which also contributes to the final weight. When the supersaturation is increased further the effect of seeding becomes apparent. For single-phase flow the net mass of crystals is up to 225 % as high for the seeded case compared to the unseeded case. For two-phase flow the increase in net crystal mass is even higher for the seeded case compared to the unseeded case. The highest average mass gain (as defined by Eder et al. [53]), 589 %, was obtained in two-phase flow seeded experiments at high supersaturation (S = 2.45).

At a relatively low supersaturation (S = 1.76) with two-phase flow and seeding we were able to obtain a net increase in the crystal mass of 6.5 mg/min without clogging, which is sufficiently high for toxicological and kinetic studies [60,61]. Assuming no clogging would occur with longer run times a net increase in the crystal mass of 9 g/day could be obtained with a single continuous microcrystallizer. This would make the developed continuous microcrystallizer suitable for on-demand manufacturing of more than 1000 doses/day of drug products with low prescribed doses (e.g. 0.5-5mg/dose) [20]. 10-20 doses of paracetamol (which is characterized by having a large prescribed dose) can be produced in a day.

Table 3. The net crystal mass (in mg) obtained at the outlet of the nucleation section (M4) for different supersaturations with their respective 95% confidence intervals.

Single-phase flow	**S = 1.22**	**S = 1.76**	**S = 2.20**	**S = 2.45**
Without seeds	10.24 ± 2.22	12.65 ± 4.06	15.74 ± 4.48	17.64 ± 1.57
With seeds	10.15 ± 4.59	17.32 ± 9.05	35.80 ± 6.51	36.85 ± 13.81
Two-phase flow				
Without seeds	10.17 ± 1.32	14.83 ± 3.63	15.12 ± 2.83	20.89 ± 6.20
With seeds	13.48 ± 3.77	39.20 ± 11.52	42.12 ± 23.05	44.61 ± 13.46

The net yield is shown in Figure 4. For all experiments, but particularly for those operated at higher supersaturations, the addition of seeds increases the net yield. The student t-test indicates that there is a statistically significant difference between the net crystal mass obtained in the seeded experiments compared to the unseeded case (for S > 1.22).

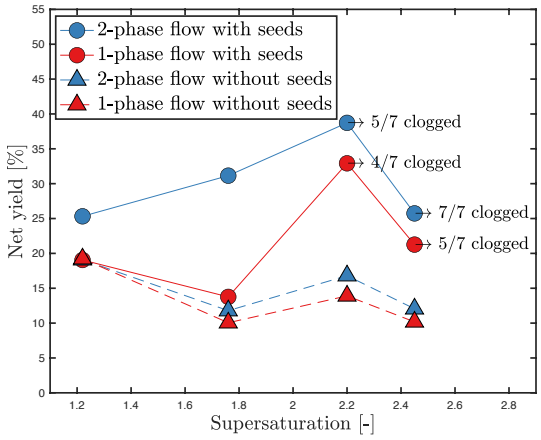

Figure 4. The net yield for varying supersaturations for seeded and unseeded cases with and without microbubbles. Experiments which were terminated before its end due to clogging are indicated in the graph. The connection lines between the data points are a guide for the eye.

Although the net crystal mass increases with increasing supersaturation, the net crystal yield initially rises while increasing supersaturation in the microcrystallizer until reaching a peak at intermediate values, after which it decreases for increasing supersaturation. This can be attributed to clogging that takes place in the microcrystallizer.

3.3 Clogging behavior

One of the major limitations of microcrystallizers is their susceptibility to clogging for flows containing solids (like crystals), which limits their continuous operation [22]. The upper operating limit of a nucleation section is the supersaturation at which nucleation and crystal growth become too dominating and clogging occurs, such that (pseudo) steady state operation is no longer feasible.

The smallest crystals in the microcrystallizer follow the streamlines caused by the bubble flow [40], as highlighted in Figure 3 (b). Large crystals, on the other hand, tend to drop to the bottom, and can get stuck on the wall. The bubbles act as a cleaning system that sweep and/or drag crystals through the channel. Figure 5 shows an example of a bubble cleaning the channel, whilst also being an attractive heterogeneous nucleation site.

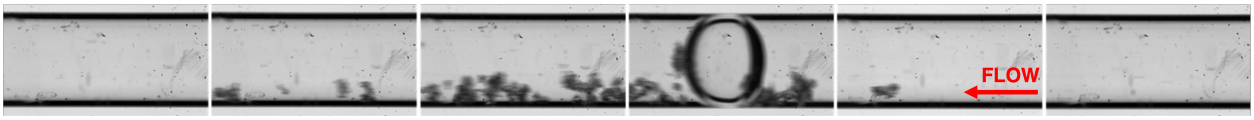

Figure 5. Nitrogen bubble cleaning the channel by sweeping away crystals stuck on the wall (S=1.76).

If too many large crystals were stuck on the wall, the bubbles are no longer able to carry them through the channel and clogging occurs. This phenomenon occurs mainly at the end of the nucleation section, where crystals are at their largest size, and for high supersaturations, for which nucleation occurs significantly faster. Figure 6 (a) and (b) shows the effect of two-phase flow in

the channel at high supersaturations: the higher number of crystals of large size in the microcrystallizer causes bubble deformation. It can be concluded that at higher supersaturations than 1.76, while the net crystal mass keeps increasing, the synergistic effect of two-phase flow and seeding becomes less apparent due to clogging. Nevertheless, a higher crystal yield with respect to the unseeded operation is always achieved. Increasing the seed loading in the microcrystallizers will increase the probabilities of clogging.

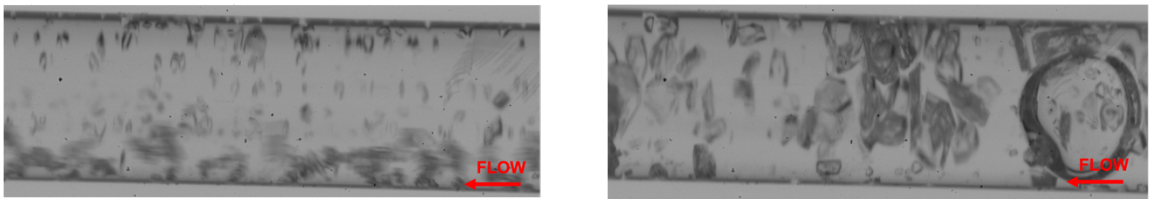

(a) (b)

Figure 6. Images of wall-attached crystals at the outlet of the microcrystallizer (ID = 1.0 mm, S = 2.45) for (a) single-phase flow with seeds, and (b) two-phase flow with seeds with a deformed microbubble.

Remarkably, two-phase flow experiments clogged faster and more often than the single-phase experiments (at high supersaturations). The extra heterogeneous nucleation sites [32] and the increased mixing causes all crystals, also those stuck on the wall, to grow faster. This can also be seen in Figure 6: crystals stuck on the wall in two-phase flow at the same conditions are significantly larger. At intermediate or low supersaturations (e.g. S=1.76 or lower) long term pseudo steady state operation can be achieved, as clogging is avoided.

3.3 Crystal size distribution

Firstly, the CSD of the outlet of the seeding section (M3) is determined for varying ultrasound conditions. Then, the CSD of the outlet of the microcrystallizers section (M1) for various

conditions is measured. Figure 7 shows the number size distribution of the seed suspension, which highlights better than a volume-based distribution whether any breakage or de-agglomeration phenomenon occurs due to the application of US. As module M3 is kept at the saturation temperature, no crystallization occurs. No relevant differences in particle size are observed. The bimodality in the 6 W curve is a post-processing artifact of the laser diffractometer. Therefore, the applied power does not cause (major) variations in the seed size distribution, prior to entering the nucleation module (M4).

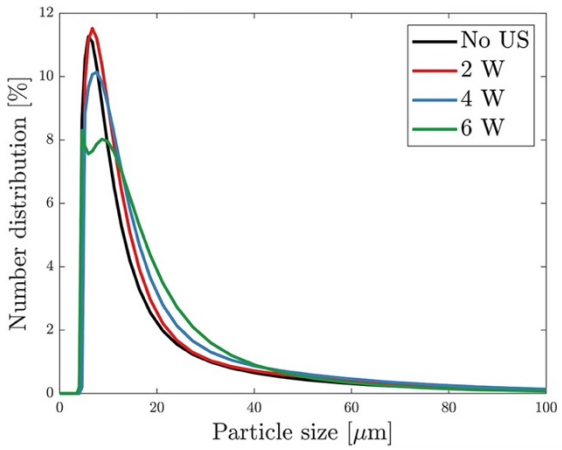

Figure 7. Number distribution of the seed suspension solution at the outlet of the seeding section (M3) for different applied power.

Figure 8 shows the CSD of the product crystals for a supersaturation of 2.45. The addition of microbubbles (using module M4) in the system decreases the mean crystal size with respect to its single-phase counterpart. The tail that appears in all distributions analysed via laser diffraction can be attributed to the agglomeration that occurs to small crystals in solution during the analysis. This is validated by the fact that the tail is not present in the number-based CSD, where agglomerates were not taken into account.

The mean crystal size increases for increasing supersaturation (as shown in supporting information figures S4 and S5), because of the increased nucleation kinetics (resulting in crystals

appearing sooner in the nucleation section), as well as increased growth kinetics (resulting in faster growth). Whilst higher nucleation rates cause a decrease in the CSD (because small crystals appear in the distribution), increases in the growth rates result in a larger CSD. In the experiments without seeds, the effect associated with the increased growth kinetics dominate if the supersaturation is increased.

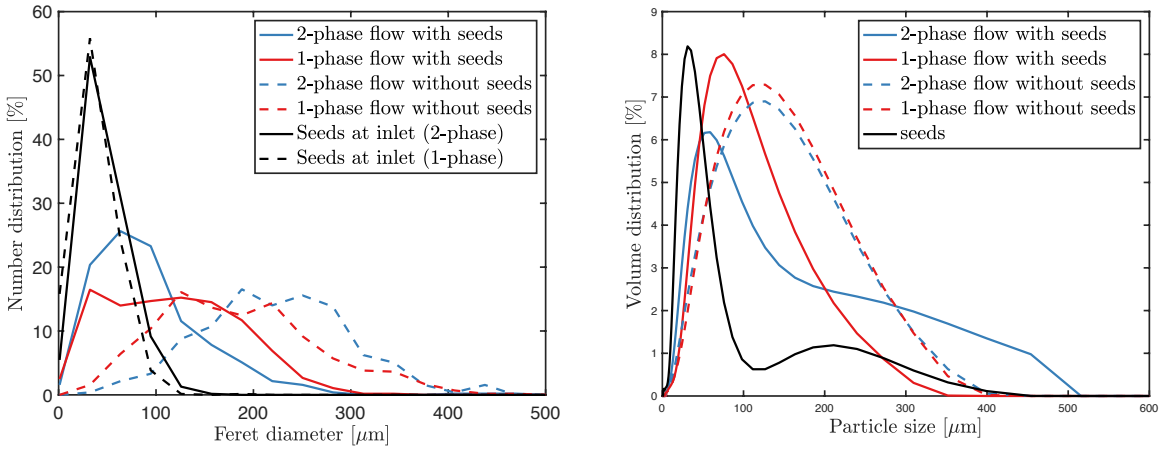

(a) (b)

Figure 8. The product crystals obtained with the application of different modular combinations in the setup (S = 2.45): (a) number-based CSD and, (b) volume-based CSD.

By adding seeds into the nucleation section, through the introduction of module M3, the (secondary) nucleation rate increases significantly. In support of this hypothesis, the SEM images show small crystals on the surface of larger crystals (Supporting Information Figure S7), which may be attributed to nuclei breeding on the surface of the parent seed crystals. The growth rate, on the other hand, is less affected by the introduction of seeds, because it does not affect the inherent growth kinetics. Hence, the CSD is shifted towards smaller crystal sizes, and the growth of crystals into very large sizes (< 350 μm) is suppressed, compared to the unseeded case (Supporting

Information Figures S4 and S5). This is evident from both the number-based and volume-based CSD, shown in Figure 8. Microscopy pictures, shown in Figure 9, show a similar trend.

The results also show that if seeds are present in the system, the supersaturation does not influence the CSD as much as without seeds. This can be attributed to the fact that the effect of supersaturation is strongly dependent on the number of crystals that are present in the microcrystallizer (module M1). If a large number of crystals is present (like in the seeded case), the supersaturation is depleted fast because of the seeds and secondary nuclei growing. These small crystals cause an increase in the surface area available for crystallization, which causes faster depletion of the supersaturation as reported by Eder et al. [53]. Without seeds the supersaturation is consumed a lot slower, because there are less crystals present in the reactor. These crystals can then continue to grow into a larger size and deplete the supersaturation without the competition of secondary nucleation.

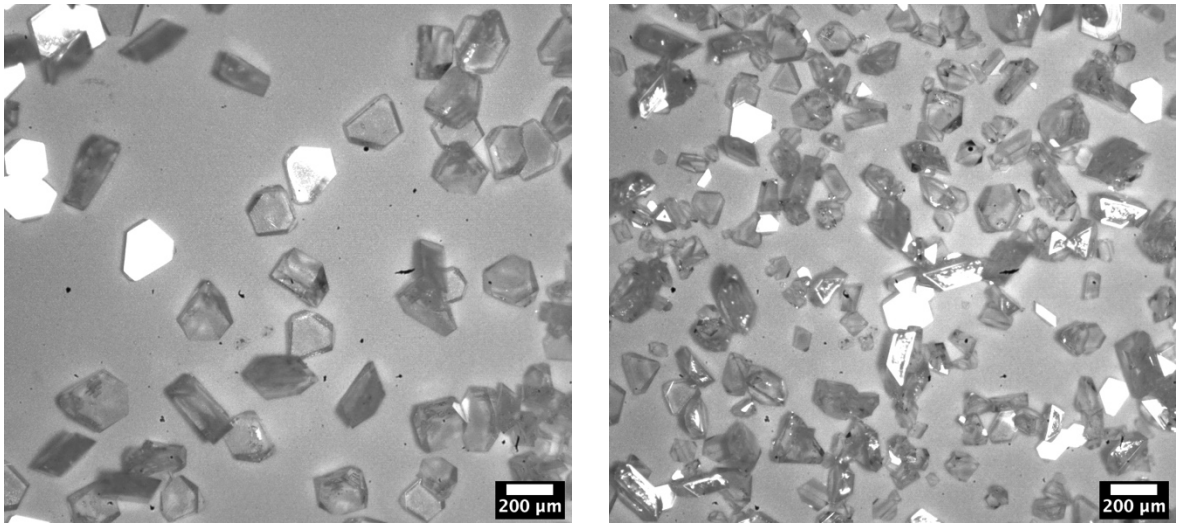

(a) (b)

Figure 9. Microscopy images from experiments (S = 2.45) for (a) single-phase flow with seeds, and (b) two-phase flow with seeds.

These results have implications for decoupling nucleation and growth in microfluidic crystallizers. In conclusion it can be said that without seeds at lower supersaturations primary nucleation is required for the appearance of the first nuclei, but growth is already the dominating crystallization mechanism (i.e. the mechanism which predominantly depletes the supersaturation). At these conditions in a small number of crystals that grow very fast after nucleation are created. The nucleation section (module M1) can be coupled to a growth section, to increase the crystal size further. By adding seeds, secondary nucleation becomes the dominating mechanism. High nucleation rates deplete the supersaturation significantly, and growth is suppressed compared to the unseeded case. This is ideal if a large number of small crystals is demanded. Also here, coupling with a growth unit would be possible, if higher yields or larger crystals are required.

CONCLUSION

We have presented a flexible microfluidic nucleation section with four different operational modes, depending on which modules are used in the setup: single-phase flow without seeds, single-phase flow with seeds, two-phase flow without seeds, and two-phase flow with seeds. To deliver the seeds to the nucleation section, a seeding module is developed, which allows off-line seed delivery, seed size and loading control. This module relies on an acoustic field to keep seeds in suspension. We have evaluated the performance of this crystallizer in terms of four interrelated properties: delivery efficiency, net yield, clogging behavior, and crystal size distribution. The delivery efficiency of the off-line produced seeds to the nucleation section is approximately 50 %, which highlights the need of proper characterization of the seed delivery methodology in continuous setups. Different supersaturations are tested, to determine the highest value at which it is possible to operate in a (pseudo) steady state whilst minimizing or avoiding clogging. An

optimal mean net yield of 38 % was obtained for a supersaturation of 2.2, with a residence time inside the nucleation unit of merely 14 s. Higher supersaturation causes earlier clogging, which eventually results in a decrease of the overall yield. Nevertheless, seeded nucleation was shown to increase the net yield for all supersaturations. When seeds are added, secondary nucleation causes a significant increase in the nucleation rate, such that the growth of the crystals is suppressed. This is reflected in the smaller crystal size distribution that is obtained for seed nucleation in comparison to nucleation without seeds. When seeds are present at higher supersaturation in two-phase flow conditions, enhanced mixing causes the seeds to grow quickly and deposit in the final section of the tubular nucleation unit, resulting in a higher clogging probability. At intermediate supersaturations the presence of microbubbles increased the net yield significantly.

ACKNOWLEDGMENT

C.D. acknowledges FWO Flanders for a Fundamental PhD fellowship (11H4421N). E.B. acknowledges FWO Flanders for a Strategic PhD fellowship (1S20023N).

ABBREVIATIONS

API active pharmaceutical ingredient; ASA acetylsalicylic acid; CD coil diameter; CFI coiled flow inverter; COBC continuous oscillatory baffled crystallizer; CSD crystal size distribution; fps frames per second; ID inner diameter; IPAc isopropyl acetate; LAM L-asparagine monohydrate; MSMPR mixed suspension mixed product removal crystallizer; OD outer diameter; PCM paracetamol; rpm rounds per minute; RTD residence time distribution; TFC tubular flow crystallizer; US ultrasound;

REFERENCES

(1) Erdemir, D.; Lee, A. Y.; Myerson, A. S. Nucleation of Crystals from Solution: Classical and Two-Step Models. *Acc. Chem. Res.* **2009**, *42* (5), 621–629. https://doi.org/10.1021/ar800217x.

(2) Lee, S.; O'Connor, T. F.; Yang, X.; Cruz, C. N.; Chatterjee, S.; Madurawe, R. D.; Moore, C. M. V.; Yu, L. X.; Woodcock, J. Modernizing Pharmaceutical Manufacturing: From Batch to Continuous Production. *J. Pharm. Innov.* **2015**, *10* (3), 191–199. https://doi.org/10.1007/s12247-015-9215-8.

(3) Ma, Y.; Wu, S.; Macaringue, E. G. J.; Zhang, T.; Gong, J.; Wang, J. Recent Progress in Continuous Crystallization of Pharmaceutical Products: Precise Preparation and Control. *Org. Process Res. Dev.* **2020**, *24* (10), 1785–1801. https://doi.org/10.1021/acs.oprd.9b00362.

(4) Lührmann, M. C.; Termühlen, M.; Timmermann, J.; Schembecker, G.; Wohlgemuth, K. Induced Nucleation by Gassing and Its Monitoring for the Design and Operation of an MSMPR Cascade. *Chem. Eng. Sci.* **2018**, *192*, 840–849. https://doi.org/10.1016/j.ces.2018.08.007.

(5) Powell, K. A.; Saleemi, A. N.; Rielly, C. D.; Nagy, Z. K. Periodic Steady-State Flow Crystallization of a Pharmaceutical Drug Using MSMPR Operation. *Chem. Eng. Process. Process Intensif.* **2015**, *97*, 195–212. https://doi.org/10.1016/j.cep.2015.01.002.

(6) Lawton, S.; Steele, G.; Shering, P.; Zhao, L.; Laird, I.; Ni, X. W. Continuous Crystallization of Pharmaceuticals Using a Continuous Oscillatory Baffled Crystallizer. *Org. Process Res.*

Dev. **2009**, *13* (6), 1357–1363. https://doi.org/10.1021/op900237x.

(7) Kacker, R.; Maaß, S.; Emmerich, J.; Kramer, H. Application of Inline Imaging for Monitoring Crystallization Process in a Continuous Oscillatory Baffled Crystallizer. *AIChE J*. **2018**, *64* (7), 2450–2461. https://doi.org/10.1002/aic.16145.

(8) Siddique, H.; Brown, C. J.; Houson, I.; Florence, A. J. Establishment of a Continuous Sonocrystallization Process for Lactose in an Oscillatory Baffled Crystallizer. *Org. Process Res. Dev*. **2015**, *19* (12), 1871–1881. https://doi.org/10.1021/acs.oprd.5b00127.

(9) Ni, X.; Liao, A. Effects of Mixing, Seeding, Material of Baffles and Final Temperature on Solution Crystallization of l-Glutamic Acid in an Oscillatory Baffled Crystallizer. *Chem. Eng. J*. **2010**, *156* (1), 226–233. https://doi.org/10.1016/j.cej.2009.10.045.

(10) McGlone, T.; Briggs, N. E. B.; Clark, C. A.; Brown, C. J.; Sefcik, J.; Florence, A. J. Oscillatory Flow Reactors (OFRs) for Continuous Manufacturing and Crystallization. *Org. Process Res. Dev*. **2015**, *19* (9), 1186–1202. https://doi.org/10.1021/acs.oprd.5b00225.

(11) Alvarez, A. J.; Myerson, A. S. Continuous Plug Flow Crystallization of Pharmaceutical Compounds. *Cryst. Growth Des*. **2010**, *10* (5), 2219–2228. https://doi.org/10.1021/cg901496s.

(12) Jiang, M.; Braatz, R. D. Designs of Continuous-Flow Pharmaceutical Crystallizers: Developments and Practice. *CrystEngComm* **2019**, *21* (23), 3534–3551. https://doi.org/10.1039/c8ce00042e.

(13) Wood, B.; Girard, K. P.; Polster, C. S.; Croker, D. M. Progress to Date in the Design and

Operation of Continuous Crystallization Processes for Pharmaceutical Applications. *Org. Process Res. Dev.* **2019**, *23* (2), 122–144. https://doi.org/10.1021/acs.oprd.8b00319.

(14) Orehek, J.; Teslić, D.; Likozar, B. Continuous Crystallization Processes in Pharmaceutical Manufacturing: A Review. *Org. Process Res. Dev.* **2021**, *25* (1), 16–42. https://doi.org/10.1021/acs.oprd.0c00398.

(15) Yazdanpanah, N.; Nagy, Z. K. *The Handbook of Continuous Crystallization*; Yazdanpanah, N., Nagy, Z. K., Eds.; Royal Society of Chemistry: Cambridge, 2020. https://doi.org/10.1039/9781788013581.

(16) Eren, A.; Civati, F.; Ma, W.; Gamekkanda, J. C.; Myerson, A. S. Continuous Crystallization and Its Potential Use in Drug Substance Manufacture : A Review. *J. Cryst. Growth* **2023**, *601* (May 2022), 126958. https://doi.org/10.1016/j.jcrysgro.2022.126958.

(17) Chen, J.; Sarma, B.; Evans, J. M. B.; Myerson, A. S. Pharmaceutical Crystallization. *Cryst. Growth Des.* **2011**, *11* (4), 887–895. https://doi.org/10.1021/cg101556s.

(18) Cogoni, G.; de Souza, B. P.; Frawley, P. J. Particle Size Distribution and Yield Control in Continuous Plug Flow Crystallizers with Recycle. *Chem. Eng. Sci.* **2015**, *138*, 592–599. https://doi.org/10.1016/j.ces.2015.08.041.

(19) Capellades, G.; Neurohr, C.; Briggs, N.; Rapp, K.; Hammersmith, G.; Brancazio, D.; Derksen, B.; Myerson, A. S. On-Demand Continuous Manufacturing of Ciprofloxacin in Portable Plug-and-Play Factories: Implementation and In Situ Control of Downstream Production. *Org. Process Res. Dev.* **2021**, *25* (7), 1534–1546. https://doi.org/10.1021/acs.oprd.1c00117.

(20) Rogers, L.; Briggs, N.; Achermann, R.; Adamo, A.; Azad, M.; Brancazio, D.; Capellades, G.; Hammersmith, G.; Hart, T.; Imbrogno, J.; Kelly, L. P.; Liang, G.; Neurohr, C.; Rapp, K.; Russell, M. G.; Salz, C.; Thomas, D. A.; Weimann, L.; Jamison, T. F.; Myerson, A. S.; Jensen, K. F. Continuous Production of Five Active Pharmaceutical Ingredients in Flexible Plug-and-Play Modules: A Demonstration Campaign. *Org. Process Res. \& Dev.* **2020**, *24* (10), 2183–2196. https://doi.org/10.1021/acs.oprd.0c00208.

(21) Dong, Z.; Wen, Z.; Zhao, F.; Kuhn, S.; Noël, T. Scale-up of Micro- and Milli-Reactors : An Overview of Strategies, Design Principles and Applications Keywords. *Chem. Eng. Sci. X* **2021**, 100097. https://doi.org/10.1016/j.cesx.2021.100097.

(22) Wu, K.; Kuhn, S. Strategies for Solids Handling in Microreactors. *Chim. Oggi/Chemistry Today* **2014**, *32* (3), 62–66.

(23) Hartman, R. L. Managing Solids in Microreactors for the Upstream Continuous Processing of Fine Chemicals. *Org. Process Res. Dev.* **2012**, *16* (5), 870–887. https://doi.org/10.1021/op200348t.

(24) Jiang, M.; Papageorgiou, C. D.; Waetzig, J.; Hardy, A.; Langston, M.; Braatz, R. D. Indirect Ultrasonication in Continuous Slug-Flow Crystallization. *Cryst. Growth Des.* **2015**, *15* (5), 2486–2492. https://doi.org/10.1021/acs.cgd.5b00263.

(25) Eder, R. J. P.; Schrank, S.; Besenhard, M. O.; Roblegg, E.; Gruber-Woelfler, H.; Khinast, J. G. Continuous Sonocrystallization of Acetylsalicylic Acid (ASA): Control of Crystal Size. *Cryst. Growth Des.* **2012**, *12* (10), 4733–4738. https://doi.org/10.1021/cg201567y.

(26) Jiang, M.; Zhu, Z.; Jimenez, E.; Papageorgiou, C. D.; Waetzig, J.; Hardy, A.; Langston, M.;

Braatz, R. D. Continuous-Flow Tubular Crystallization in Slugs Spontaneously Induced by Hydrodynamics. *Cryst. Growth Des.* **2014**, *14* (2), 851–860. https://doi.org/10.1021/cg401715e.

(27) Termühlen, M.; Etmanski, M. M.; Kryschewski, I.; Kufner, A. C.; Schembecker, G.; Wohlgemuth, K. Continuous Slug Flow Crystallization: Impact of Design and Operating Parameters on Product Quality. *Chem. Eng. Res. Des.* **2021**, *170*, 290–303. https://doi.org/10.1016/j.cherd.2021.04.006.

(28) Neugebauer, P.; Khinast, J. G. Continuous Crystallization of Proteins in a Tubular Plug-Flow Crystallizer. *Cryst. Growth Des.* **2015**, *15* (3), 1089–1095. https://doi.org/10.1021/cg501359h.

(29) Rossi, D.; Gavriilidis, A.; Kuhn, S.; Candel, M. A.; Jones, A. G.; Price, C.; Mazzei, L. Adipic Acid Primary Nucleation Kinetics from Probability Distributions in Droplet-Based Systems under Stagnant and Flow Conditions. *Cryst. Growth Des.* **2015**, *15* (4), 1784–1791. https://doi.org/10.1021/cg501836e.

(30) Robertson, K.; Flandrin, P. B.; Klapwijk, A. R.; Wilson, C. C. Design and Evaluation of a Mesoscale Segmented Flow Reactor (KRAIC). *Cryst. Growth Des.* **2016**, *16* (8), 4759–4764. https://doi.org/10.1021/acs.cgd.6b00885.

(31) Warnier, M. J. F. *Taylor Flow Hydrodynamics in Gas-Liquid-Solid Micro Reactors*; 2009; Vol. 1. https://doi.org/10.6100/IR653976.

(32) Fatemi, N.; Dong, Z.; Van Gerven, T.; Kuhn, S. Microbubbles as Heterogeneous Nucleation Sites for Crystallization in Continuous Microfluidic Devices. *Langmuir* **2019**, *35* (1), 60–

69. https://doi.org/10.1021/acs.langmuir.8b03183.

(33) Delacour, C.; Lutz, C.; Kuhn, S. Pulsed Ultrasound for Temperature Control and Clogging Prevention in Micro-Reactors. *Ultrason. Sonochem.* **2019**, *55* (November 2018), 67–74. https://doi.org/10.1016/j.ultsonch.2019.03.012.

(34) Devos, C.; Van Gerven, T.; Kuhn, S. Nucleation Kinetics for Primary, Secondary and Ultrasound-Induced Paracetamol Crystallization. *CrystEngComm* **2021**, *23* (30), 5164–5175. https://doi.org/10.1039/D1CE00676B.

(35) Ruecroft, G.; Hipkiss, D.; Ly, T.; Maxted, N.; Cains, P. W. Sonocrystallization : The Use of Ultrasound for Improved Industrial Crystallization Abstract : *Org. Process Res. Dev.* **2005**, *9* (6), 923–932.

(36) Gielen, B.; Claes, T.; Janssens, J.; Jordens, J.; Thomassen, L. C. J.; Gerven, T. Van; Braeken, L. Particle Size Control during Ultrasonic Cooling Crystallization of Paracetamol. *Chem. Eng. Technol.* **2017**, *40* (7), 1300–1308. https://doi.org/10.1002/ceat.201600647.

(37) Fatemi, N.; Devos, C.; Van Gerven, T.; Kuhn, S. Continuous Crystallization of Paracetamol Exploiting Gas-Liquid Flow in Modular Nucleation and Growth Stages. *Chem. Eng. Sci.* **2021**, *248*, 117095. https://doi.org/10.1016/j.ces.2021.117095.

(38) Devos, C.; Van Gerven, T.; Kuhn, S. A Review of Experimental Methods for Nucleation Rate Determination in Large-Volume Batch and Microfluidic Crystallization. *Cryst. Growth Des.* **2021**, *21* (4), 2541–2565. https://doi.org/10.1021/acs.cgd.0c01606.

(39) He, Y.; Gao, Z.; Zhang, T.; Sun, J.; Ma, Y.; Tian, N.; Gong, J. Seeding Techniques and

Optimization of Solution Crystallization Processes. *Org. Process Res. Dev.* **2020**, *24* (10), 1839–1849. https://doi.org/10.1021/acs.oprd.0c00151.

(40) Paul, E. L.; Tung, H.-H.; Midler, M. Organic Crystallization Processes. *Powder Technol.* **2005**, *150* (2), 133–143. https://doi.org/10.1016/j.powtec.2004.11.040.

(41) Agrawal, S. G.; Paterson, A. H. J. Secondary Nucleation: Mechanisms and Models. *Chem. Eng. Commun.* **2015**, *202* (5), 698–706. https://doi.org/10.1080/00986445.2014.969369.

(42) Jordens, J.; Canini, E.; Gielen, B.; Van Gerven, T.; Braeken, L. Ultrasound Assisted Particle Size Control by Continuous Seed Generation and Batch Growth. *Crystals* **2017**, *7* (7). https://doi.org/10.3390/cryst7070195.

(43) Han, B.; Ezeanowi, N. C.; Koiranen, T. O.; Häkkinen, A. T.; Louhi-Kultanen, M. Insights into Design Criteria for a Continuous, Sonicated Modular Tubular Cooling Crystallizer. *Cryst. Growth Des.* **2018**, *18* (12), 7286–7295. https://doi.org/10.1021/acs.cgd.8b00700.

(44) Rimez, B.; Debuysschère, R.; Conté, J.; Lecomte-Norrant, E.; Gourdon, C.; Cognet, P.; Scheid, B. Continuous-Flow Tubular Crystallization to Discriminate between Two Competing Crystal Polymorphs. 1. Cooling Crystallization. *Cryst. Growth Des.* **2018**, *18* (11), 6431–6439. https://doi.org/10.1021/acs.cgd.8b00928.

(45) Rimez, B.; Debuysschère, R.; Scheid, B. On the Effect of Flow Restrictions on the Nucleation Behavior of Molecules in Tubular Flow Nucleators. *J. Flow Chem.* **2020**, *10* (1), 241–249. https://doi.org/10.1007/s41981-019-00069-2.

(46) Klutz, S.; Kurt, S. K.; Lobedann, M.; Kockmann, N. Narrow Residence Time Distribution

in Tubular Reactor Concept for Reynolds Number Range of 10-100. *Chem. Eng. Res. Des.* **2015**, *95*, 22–33. https://doi.org/10.1016/j.cherd.2015.01.003.

(47) Hohmann, L.; Greinert, T.; Mierka, O.; Turek, S.; Schembecker, G.; Bayraktar, E.; Wohlgemuth, K.; Kockmann, N. Analysis of Crystal Size Dispersion Effects in a Continuous Coiled Tubular Crystallizer: Experiments and Modeling. *Cryst. Growth Des.* **2018**, *18* (3), 1459–1473. https://doi.org/10.1021/acs.cgd.7b01383.

(48) Rossi, D.; Gargiulo, L.; Valitov, G.; Gavriilidis, A.; Mazzei, L. Experimental Characterization of Axial Dispersion in Coiled Flow Inverters. *Chem. Eng. Res. Des.* **2017**, *120*, 159–170. https://doi.org/10.1016/j.cherd.2017.02.011.

(49) Hohmann, L.; Gorny, R.; Klaas, O.; Ahlert, J.; Wohlgemuth, K.; Kockmann, N. Design of a Continuous Tubular Cooling Crystallizer for Process Development on Lab-Scale. *Chem. Eng. Technol.* **2016**, *39* (7), 1268–1280. https://doi.org/10.1002/ceat.201600072.

(50) Schmalenberg, M.; Weick, L. K.; Kockmann, N. Nucleation in Continuous Flow Cooling Sonocrystallization for Coiled Capillary Crystallizers. *J. Flow Chem.* **2021**, *11* (3), 303–319. https://doi.org/10.1007/s41981-020-00138-x.

(51) Méndez Del Río, J. R.; Rousseau, R. W. Batch and Tubular-Batch Crystallization of Paracetamol: Crystal Size Distribution and Polymorph Formation. *Cryst. Growth Des.* **2006**, *6* (6), 1407–1414. https://doi.org/10.1021/cg060025v.

(52) Eder, R. J. P.; Radl, S.; Schmitt, E.; Innerhofer, S.; Maier, M.; Gruber-Woelfler, H.; Khinast, J. G. Continuously Seeded, Continuously Operated Tubular Crystallizer for the Production of Active Pharmaceutical Ingredients. *Cryst. Growth Des.* **2010**, *10* (5), 2247–2257.

https://doi.org/10.1021/cg9015788.

(53) Eder, R. J. P.; Schmitt, E. K.; Grill, J.; Radl, S.; Gruber-Woelfler, H.; Khinast, J. G. Seed Loading Effects on the Mean Crystal Size of Acetylsalicylic Acid in a Continuous-Flow Crystallization Device. *Cryst. Res. Technol.* **2011**, *46* (3), 227–237. https://doi.org/10.1002/crat.201000634.

(54) Wong, S. Y.; Cui, Y.; Myerson, A. S. Contact Secondary Nucleation as a Means of Creating Seeds for Continuous Tubular Crystallizers. *Cryst. Growth Des.* **2013**, *13* (6), 2514–2521. https://doi.org/10.1021/cg4002303.

(55) Besenhard, M. O.; Neugebauer, P.; Ho, C. Da; Khinast, J. G. Crystal Size Control in a Continuous Tubular Crystallizer. *Cryst. Growth Des.* **2015**, *15* (4), 1683–1691. https://doi.org/10.1021/cg501637m.

(56) Fujiwara, M.; Chow, P. S.; Ma, D. L.; Braatz, R. D. Paracetamol Crystallization Using Laser Backscattering and ATR-FTIR Spectroscopy: Metastability, Agglomeration and Control. *Cryst. Growth Des.* **2002**, *2* (5), 363–370.

(57) Dong, Z.; Fernandez Rivas, D.; Kuhn, S. Acoustophoretic Focusing Effects on Particle Synthesis and Clogging in Microreactors. *Lab Chip* **2019**, *19* (2), 316–327. https://doi.org/10.1039/C8LC00675J.

(58) Beckmann, W.; Nickisch, K.; Budde, U. Development of a Seeding Technique for the Crystallization of the Metastable a Modification of Abecarnil. *Org. Process Res. Dev.* **1998**, *2* (5), 298–304. https://doi.org/10.1021/op980029b.

(59) Besenhard, M. O.; Hohl, R.; Hodzic, A.; Eder, R. J. P.; Khinast, J. G. Modeling a Seeded Continuous Crystallizer for the Production of Active Pharmaceutical Ingredients. *Cryst. Res. Technol.* **2014**, *49* (2–3), 92–108. https://doi.org/10.1002/crat.201300305.

(60) Plouffe, P.; Bittel, M.; Sieber, J.; Roberge, D. M.; Macchi, A. On the Scale-up of Micro-Reactors for Liquid-Liquid Reactions. *Chem. Eng. Sci.* **2016**, *143*, 216–225. https://doi.org/10.1016/j.ces.2015.12.009.

(61) Malet-Sanz, L.; Susanne, F. Continuous Flow Synthesis. a Pharma Perspective. *J. Med. Chem.* **2012**, *55* (9), 4062–4098. https://doi.org/10.1021/jm2006029.

SUPPLEMENTARY INFORMATION

Characterization of a modular microfluidic section for seeded nucleation in multiphase flow

Cedric Devos [a‡], *Elena Brozzi* [a‡], *Tom Van Gerven* [a], *and Simon Kuhn* [a*]

[a] *KU Leuven, Department of Chemical Engineering, 3001 Leuven, Belgium*

[*] Email: simon.kuhn@kuleuven.be

[‡] *C.D. and E.B. contributed equally to this paper.*

S1. Coiled crystallizers in literature

TFCs are coiled to reduce the operational space and to improve mixing. More recently, also coiled flow inverter (CFI) crystallizers have been used to further enhance the effects of coiling [1–4]. Table S1 gives a selected overview of coiled crystallizers in literature.

Table S1 Selected overview of the use of coiled tubular crystallizers in literature, and coiled flow inverters (CFI). * refers to anti-solvent crystallization.

	Coil	Coil orientation	Coil diameter
Present work	**No**	-	-
Jiang et al. (2015) [5]	No	-	-
Termühlen et al. (2021) [6]	No	-	-
Mou et al. (2020) [7]	No	-	-
Méndez Del Río and Rousseau (2020) [8]	Yes	Horizontal	N/A
Eder et al. (2010, 2011, 2012) [9–11]	Yes	Vertical, horizontal	CD=100 mm
Jiang et al. (2014) [12]	Yes	Horizontal	N/A
Rossi et al. (2015) [13]	Yes	Vertical	N/A
Besenhard et al. (2015) [14]	Yes	Horizontal	CD=100 mm
Neugebauer et al. (2015) [15]	Yes	Vertical	CD=215 mm
Robertson et al. (2016) [16]	Yes	Horizontal	N/A
Wiedmeyer et al. (2017) [17]	Yes	Horizontal	CD=115 mm
Han et al. (2018) [18]	Yes	Horizontal	CD=95, 105 mm
Hadiwinoto et al. (2019) [19] *	Yes	Horizontal	N/A
Fatemi et al. (2021) [20]	Yes	Vertical	CD=20 mm
Klutz et al. (2015) [1]	Yes	CFI (3, 15, 27 bends)	CD=63 mm
Rossi et al. (2017) [2]	Yes	CFI (19 bends)	CD=17, 20, 32 mm
Hohmann et al. (2016) [3]	Yes	CFI (8 bends)	CD=41 mm
Hohmann et al. (2018) [21]	Yes	CFI (8 bends)	CD=41 mm
Schmalenberg et al. (2021) [4]	Yes	CFI (6 bends)	CD=52 mm
Schmalenberg et al. (2021) [22]	Yes	CFI (4 bends/unit, 7 units)	CD=40 mm

S2. Temperature measurements

The experimentally measured temperatures in the seeding section and the position of the thermocouples in the system are shown in Figure S1.

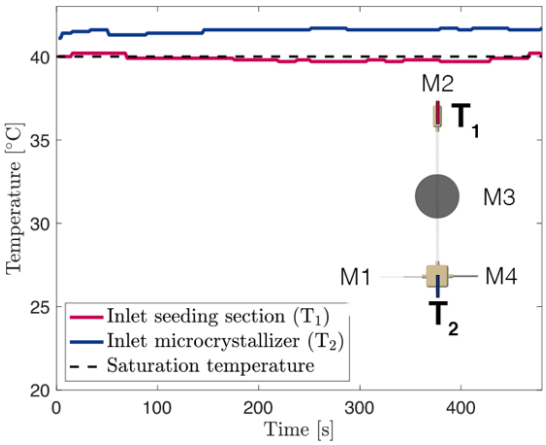

Figure S1 Temperature measurements at the inlet of the seeding section (M3) and the inlet of the microcrystallizer (M4).

S3. Solid loading

The solid loading mass fraction in the crystallizer can be calculated using eq. S1 [21], in which w_{susp} and w_{sol} refer to the weight concentration of the seeds respectively in the suspension and in the solution [21].

$$X_{seeds} = \frac{w_{susp}}{(1 - w_{susp})(1 - w_{sol})} \quad (S1)$$

The theoretical crystallizable mass fraction in the system is dependent on the supersaturation (S) applied, and it is estimated using eq. S2, with w_{sat} the PCM mass in $g \cdot g^{-1}$ solution at the saturation temperature [21].

$$X_{prod,S} = \left(\frac{w_{sat}}{1 - w_{sat}}\right)_{T_{in}} - \left(\frac{w_{sat}}{1 - w_{sat}}\right)_{T_{out}} \quad (S2)$$

The total seed loading at a specific supersaturation (S) can be eventually estimated by referring to the crystallizing solution with eq. S3 [10,23]. Table S2 contains the solid loading as a function of S for all conditions applied in this work.

$$\text{Seed loading } [\%] = \frac{X_{seeds}}{X_{prod,S}} \cdot 100 \quad (S3)$$

Table S2 Seed loading of the system for different supersaturations inside the crystallizer.

	S = 1.22	S = 1.76	S = 2.20	S = 2.45
Seed loading [%]	135.4	74.0	58.5	53.9

S4. Volume-based size distribution

Figures S2 and Figure S3 show the volume-based crystal size distributions (CSD) for setups with varying modules installed, for varying supersaturations. The seeds distribution shown in these figures is the size of the dry and sieved seeds.

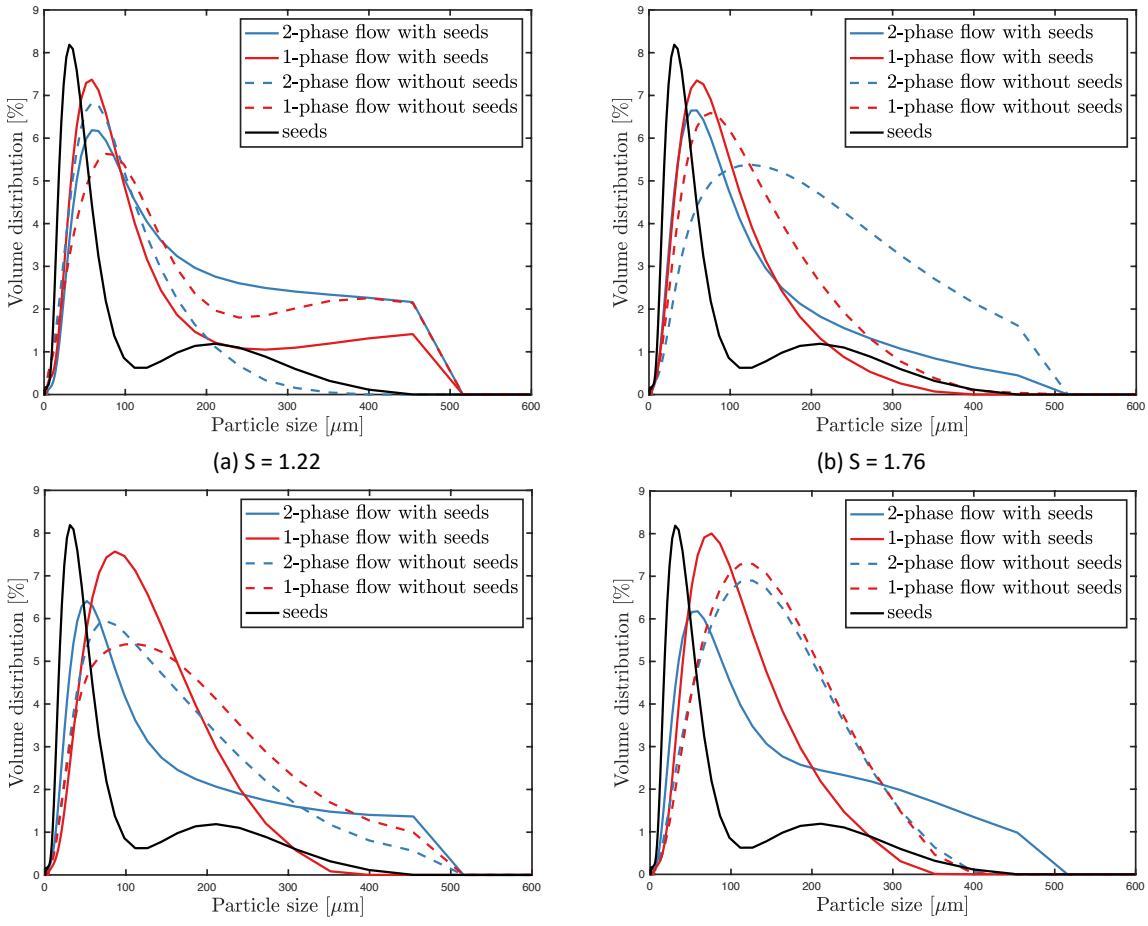

(a) S = 1.22 (b) S = 1.76

(c) S = 2.20 (d) S = 2.45

Figure S2 CSD (volume-based) of the product crystals obtained with the application of different modular combinations in the setup, for different supersaturation in the crystallizer.

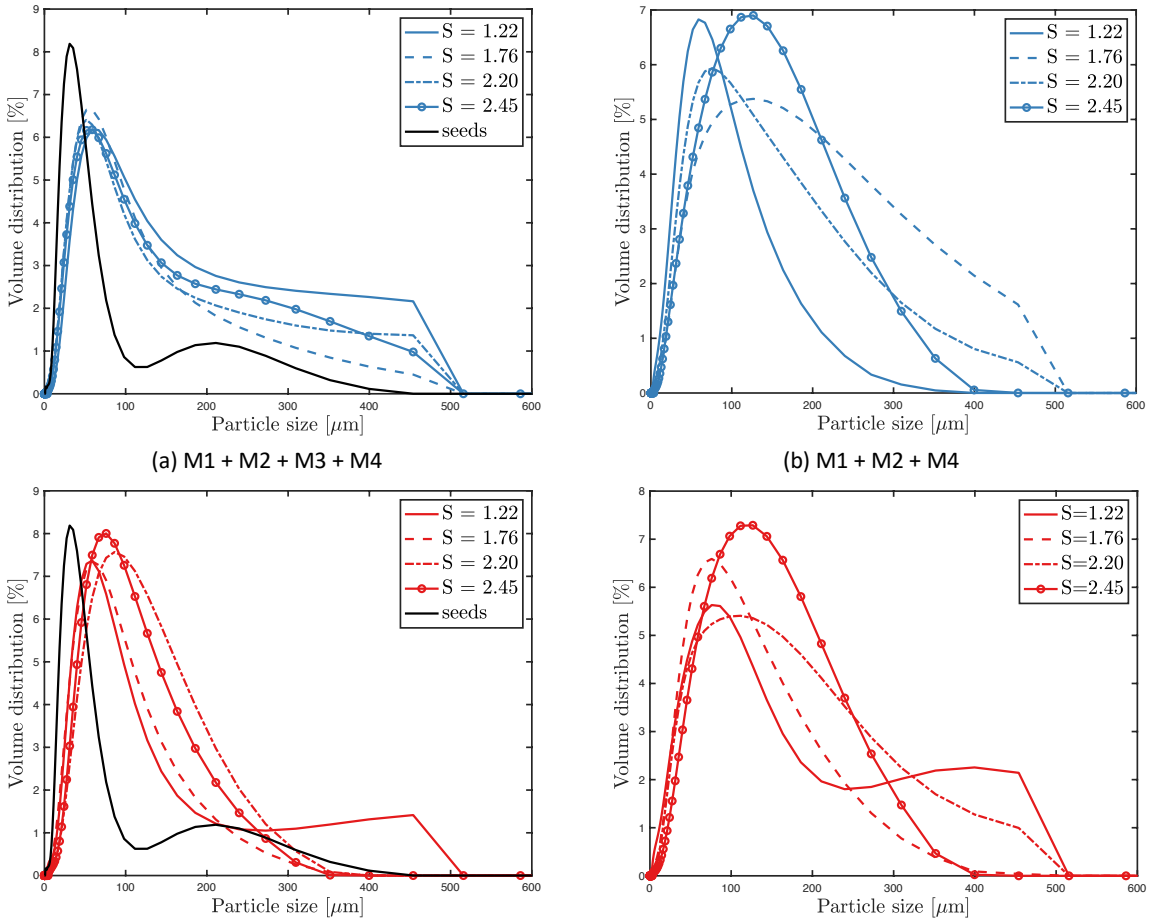

Figure S3 Comparison of the CSD (volume-based) for different supersaturations when the same modular combination is applied.

S5. Number-based size distribution

Figure S4 shows the crystals obtained at the inlet of the microcrystallizer, which are the seed crystals, and the crystals at the outlet of the microcrystallizer. Figures S5 and Figure S6 show the mass-based crystal size distributions (CSD) for setups with varying modules installed, for varying supersaturations. Also in these curves the seeds at the inlet of the microcrystallizer are shown.

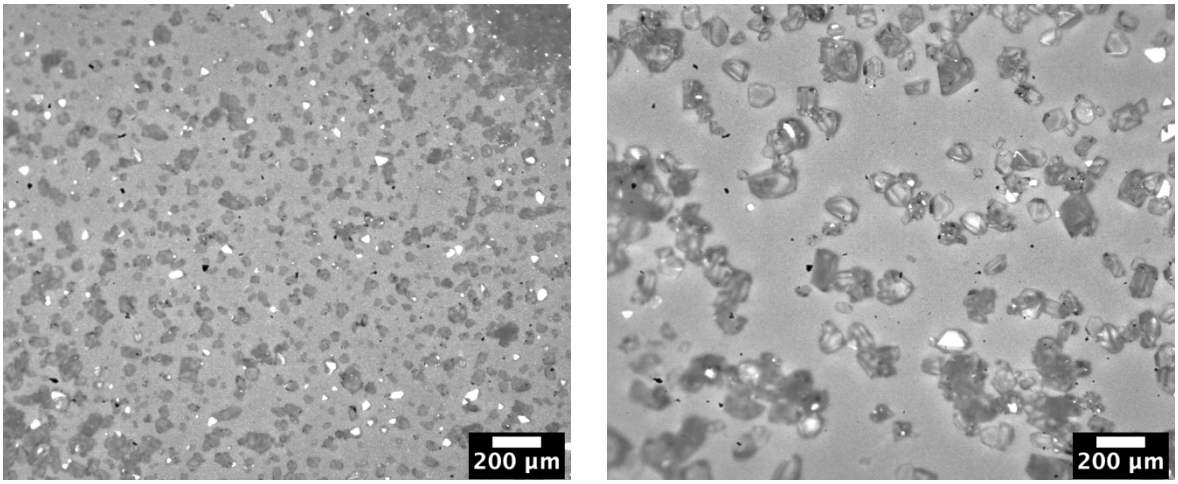

(a) (b)

Figure S4 Microscopy images from experiments with Modules M1 + M2 + M3 + M4 installed (two-phase flow with seeds) for (a) the inlet of the microcrystallizer (S = 1.00), and (b) the outlet of the microcrystallizer (S = 1.22).

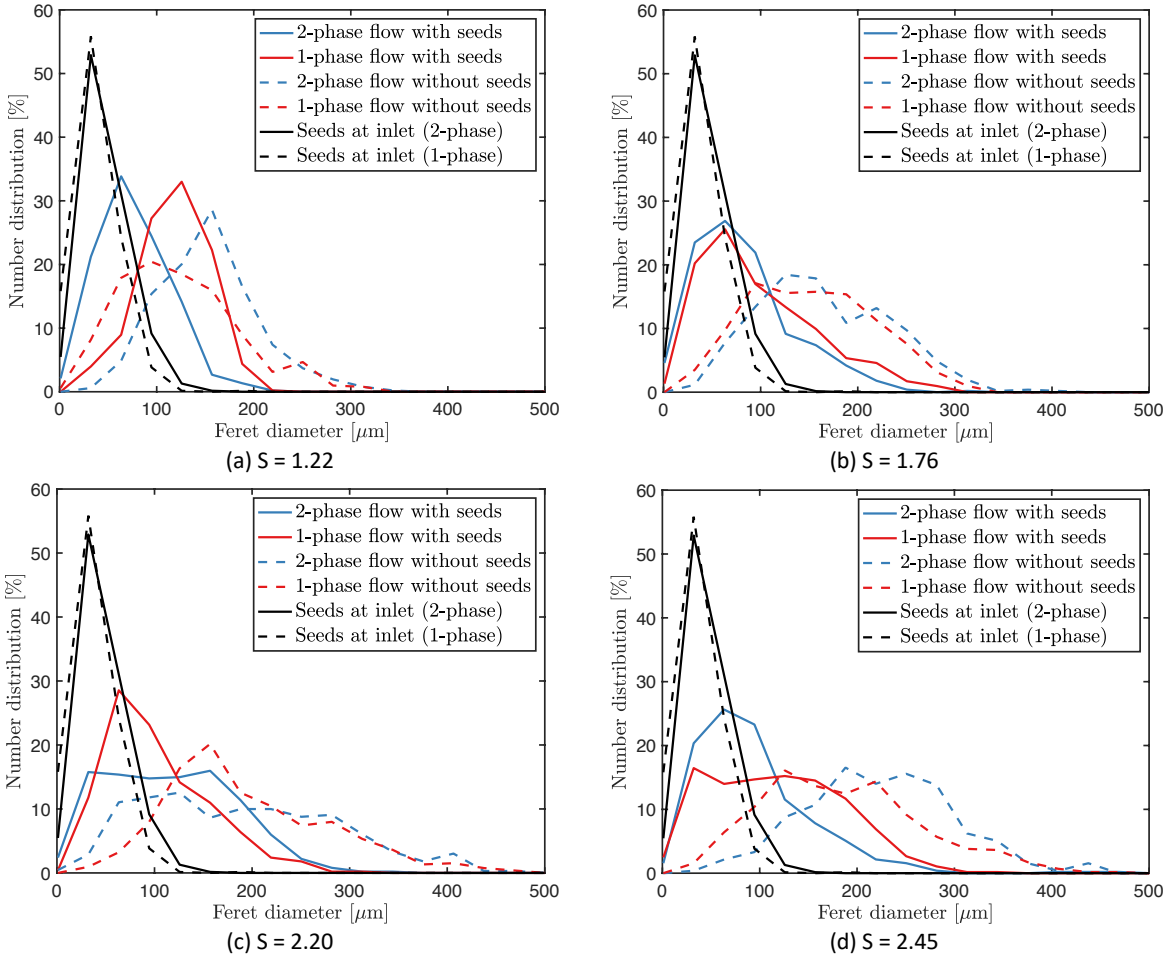

(a) S = 1.22 (b) S = 1.76

(c) S = 2.20 (d) S = 2.45

Figure S5 CSD (number-based) of the product crystals obtained with the application of different modular combinations in the setup, for different supersaturation in the crystallizer.

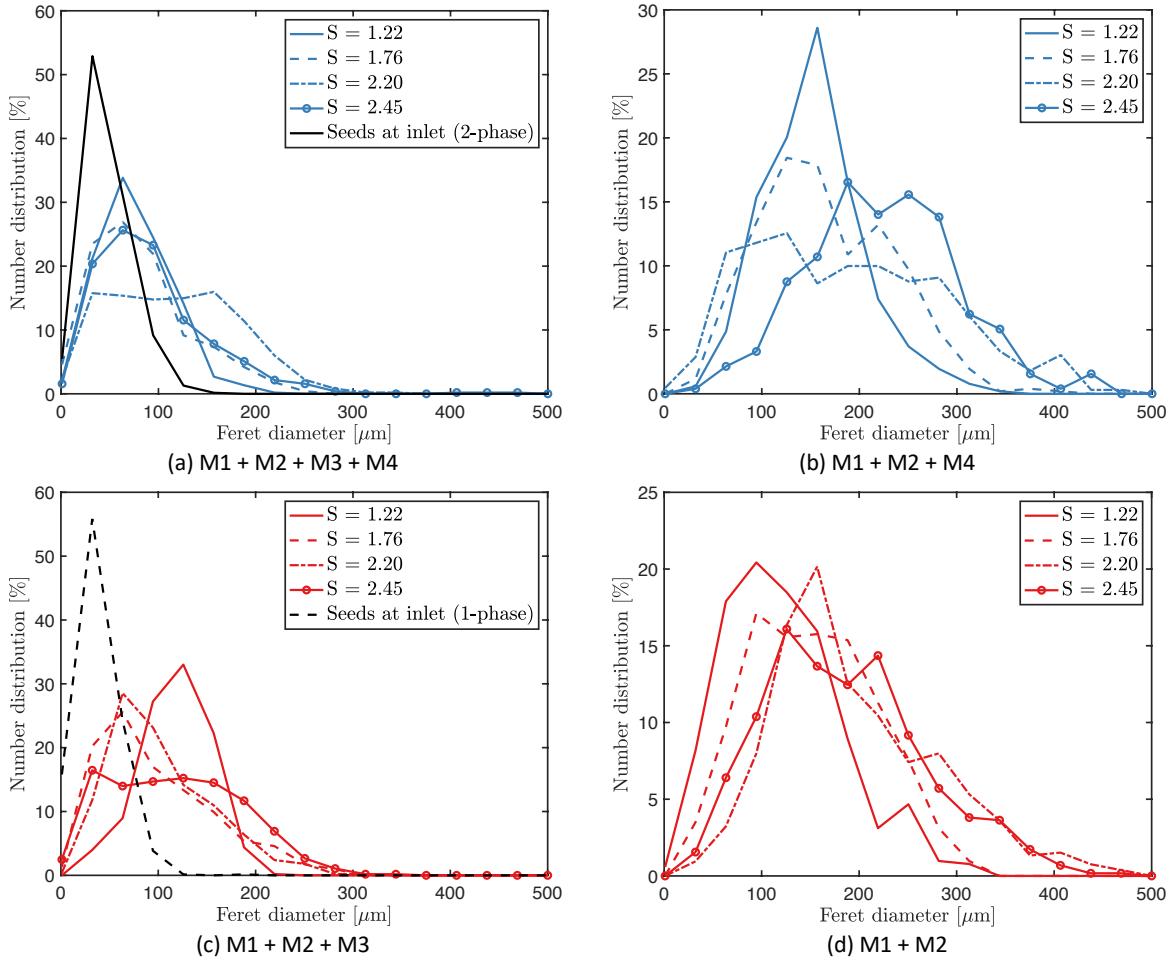

Figure S6 Comparison of the CSD (number-based) for different supersaturations when the same modular combination is applied.

S6. Crystal surface

Scanning electron microscopy pictures of the surface of the crystals show that small nuclei are present on the surface of larger crystals, as shown in Figure S7. Nevertheless, no conclusions could be made based on these images.

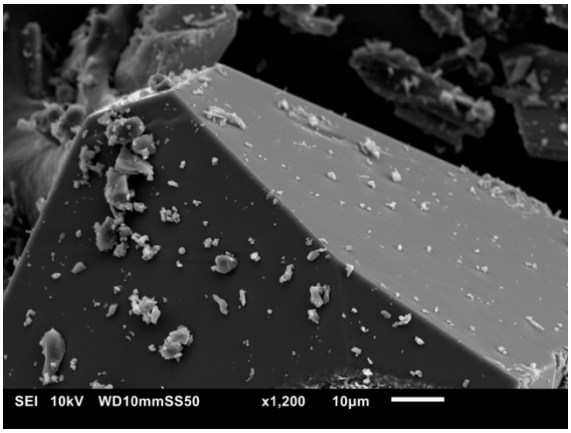

Figure S7 SEM image of the surface of a large seed crystal, from a two-phase flow seeded experiment (S=1.76).

S7. Oscillating flow

The oscillation flow was obtained by increasing the flow rate of the VICI M6 piston pump, which delivers the solution, four times for 1.5 s every minute. The total mean cumulative flow rate was kept constant throughout the experiment (2.0 mL/min). Also, the suspension flow rate was kept constant at 0.5 mL/min.

Table S3 The flow rates (in mL/min) that were used in the experiments for varying oscillation flow rates.

Pulse flow rate	Suspension flow rate	Solution flow rate	Total mean cumulative flow rate
0.00	0.50	1.50	2.00
2.50	0.50	1.39	2.00
5.00	0.50	1.11	2.00

References

(1) Klutz, S.; Kurt, S. K.; Lobedann, M.; Kockmann, N. Narrow Residence Time Distribution in Tubular Reactor Concept for Reynolds Number Range of 10-100. *Chem. Eng. Res. Des.* **2015**, *95*, 22–33. https://doi.org/10.1016/j.cherd.2015.01.003.

(2) Rossi, D.; Gargiulo, L.; Valitov, G.; Gavriilidis, A.; Mazzei, L. Experimental Characterization of Axial Dispersion in Coiled Flow Inverters. *Chem. Eng. Res. Des.* **2017**, *120*, 159–170. https://doi.org/10.1016/j.cherd.2017.02.011.

(3) Hohmann, L.; Gorny, R.; Klaas, O.; Ahlert, J.; Wohlgemuth, K.; Kockmann, N. Design of a Continuous Tubular Cooling Crystallizer for Process Development on Lab-Scale. *Chem. Eng. Technol.* **2016**, *39* (7), 1268–1280. https://doi.org/10.1002/ceat.201600072.

(4) Schmalenberg, M.; Weick, L. K.; Kockmann, N. Nucleation in Continuous Flow Cooling Sonocrystallization for Coiled Capillary Crystallizers. *J. Flow Chem.* **2021**, *11* (3), 303–319. https://doi.org/10.1007/s41981-020-00138-x.

(5) Jiang, M.; Papageorgiou, C. D.; Waetzig, J.; Hardy, A.; Langston, M.; Braatz, R. D. Indirect Ultrasonication in Continuous Slug-Flow Crystallization. *Cryst. Growth Des.* **2015**, *15* (5), 2486–2492. https://doi.org/10.1021/acs.cgd.5b00263.

(6) Termühlen, M.; Etmanski, M. M.; Kryschewski, I.; Kufner, A. C.; Schembecker, G.; Wohlgemuth, K. Continuous Slug Flow Crystallization: Impact of Design and Operating Parameters on Product Quality. *Chem. Eng. Res. Des.* **2021**, *170*, 290–303. https://doi.org/10.1016/j.cherd.2021.04.006.

(7) Mou, M.; Jiang, M. Fast Continuous Non-Seeded Cooling Crystallization of Glycine in Slug Flow: Pure α-Form Crystals with Narrow Size Distribution. *J. Pharm. Innov.* **2020**, *15* (2), 281–294. https://doi.org/10.1007/s12247-020-09438-0.

(8) Méndez Del Río, J. R.; Rousseau, R. W. Batch and Tubular-Batch Crystallization of Paracetamol: Crystal Size Distribution and Polymorph Formation. *Cryst. Growth Des.* **2006**, *6* (6), 1407–1414. https://doi.org/10.1021/cg060025v.

(9) Eder, R. J. P.; Radl, S.; Schmitt, E.; Innerhofer, S.; Maier, M.; Gruber-Woelfler, H.; Khinast, J. G. Continuously Seeded, Continuously Operated Tubular Crystallizer for the Production of Active Pharmaceutical Ingredients. *Cryst. Growth Des.* **2010**, *10* (5), 2247–2257. https://doi.org/10.1021/cg9015788.

(10) Eder, R. J. P.; Schmitt, E. K.; Grill, J.; Radl, S.; Gruber-Woelfler, H.; Khinast, J. G. Seed Loading Effects on the Mean Crystal Size of Acetylsalicylic Acid in a Continuous-Flow Crystallization Device. *Cryst. Res. Technol.* **2011**, *46* (3), 227–237. https://doi.org/10.1002/crat.201000634.

(11) Eder, R. J. P.; Schrank, S.; Besenhard, M. O.; Roblegg, E.; Gruber-Woelfler, H.; Khinast, J. G. Continuous Sonocrystallization of Acetylsalicylic Acid (ASA): Control of Crystal Size. *Cryst.*

Growth Des. **2012**, *12* (10), 4733–4738. https://doi.org/10.1021/cg201567y.
(12) Jiang, M.; Zhu, Z.; Jimenez, E.; Papageorgiou, C. D.; Waetzig, J.; Hardy, A.; Langston, M.; Braatz, R. D. Continuous-Flow Tubular Crystallization in Slugs Spontaneously Induced by Hydrodynamics. *Cryst. Growth Des.* **2014**, *14* (2), 851–860. https://doi.org/10.1021/cg401715e.
(13) Rossi, D.; Gavriilidis, A.; Kuhn, S.; Candel, M. A.; Jones, A. G.; Price, C.; Mazzei, L. Adipic Acid Primary Nucleation Kinetics from Probability Distributions in Droplet-Based Systems under Stagnant and Flow Conditions. *Cryst. Growth Des.* **2015**, *15* (4), 1784–1791. https://doi.org/10.1021/cg501836e.
(14) Besenhard, M. O.; Neugebauer, P.; Ho, C. Da; Khinast, J. G. Crystal Size Control in a Continuous Tubular Crystallizer. *Cryst. Growth Des.* **2015**, *15* (4), 1683–1691. https://doi.org/10.1021/cg501637m.
(15) Neugebauer, P.; Khinast, J. G. Continuous Crystallization of Proteins in a Tubular Plug-Flow Crystallizer. *Cryst. Growth Des.* **2015**, *15* (3), 1089–1095. https://doi.org/10.1021/cg501359h.
(16) Robertson, K.; Flandrin, P. B.; Klapwijk, A. R.; Wilson, C. C. Design and Evaluation of a Mesoscale Segmented Flow Reactor (KRAIC). *Cryst. Growth Des.* **2016**, *16* (8), 4759–4764. https://doi.org/10.1021/acs.cgd.6b00885.
(17) Wiedmeyer, V.; Anker, F.; Bartsch, C.; Voigt, A.; John, V.; Sundmacher, K. Continuous Crystallization in a Helically Coiled Flow Tube: Analysis of Flow Field, Residence Time Behavior, and Crystal Growth. *Ind. Eng. Chem. Res.* **2017**, *56* (13), 3699–3712. https://doi.org/10.1021/acs.iecr.6b04279.
(18) Han, B.; Ezeanowi, N. C.; Koiranen, T. O.; Häkkinen, A. T.; Louhi-Kultanen, M. Insights into Design Criteria for a Continuous, Sonicated Modular Tubular Cooling Crystallizer. *Cryst. Growth Des.* **2018**, *18* (12), 7286–7295. https://doi.org/10.1021/acs.cgd.8b00700.
(19) Hadiwinoto, G. D.; Kwok, P. C. L.; Tong, H. H. Y.; Wong, S. N.; Chow, S. F.; Lakerveld, R. Integrated Continuous Plug-Flow Crystallization and Spray Drying of Pharmaceuticals for Dry Powder Inhalation. *Ind. Eng. Chem. Res.* **2019**, *58* (36), 16843–16857. https://doi.org/10.1021/acs.iecr.9b01730.
(20) Fatemi, N.; Devos, C.; Van Gerven, T.; Kuhn, S. Continuous Crystallization of Paracetamol Exploiting Gas-Liquid Flow in Modular Nucleation and Growth Stages. *Chem. Eng. Sci.* **2021**, *248*, 117095. https://doi.org/10.1016/j.ces.2021.117095.
(21) Hohmann, L.; Greinert, T.; Mierka, O.; Turek, S.; Schembecker, G.; Bayraktar, E.; Wohlgemuth, K.; Kockmann, N. Analysis of Crystal Size Dispersion Effects in a Continuous Coiled Tubular Crystallizer: Experiments and Modeling. *Cryst. Growth Des.* **2018**, *18* (3), 1459–1473. https://doi.org/10.1021/acs.cgd.7b01383.
(22) Schmalenberg, M.; Kreis, S.; Weick, L. K.; Haas, C.; Sallamon, F.; Kockmann, N. Continuous Cooling Crystallization in a Coiled Flow Inverter Crystallizer Technology—Design, Characterization, and Hurdles. *Processes* **2021**, *9* (9), 1537. https://doi.org/10.3390/pr9091537.
(23) Roberts, K. J.; Docherty, R.; Tamura, R. *Engineering Crystallography: From Molecule to Crystal to Functional Form*; Roberts, K. J., Docherty, R., Tamura, R., Eds.; NATO Science for Peace and Security Series A: Chemistry and Biology; Springer Netherlands: Dordrecht, 2017. https://doi.org/10.1007/978-94-024-1117-1.